Euler Solutions for Transonic Flow Past a Fighter Wing

L. N. Sankar*
Georgia Institute of Technology, Atlanta, Georgia
and
J. B. Malone† and D. Schuster‡
Lockheed Georgia Company, Marietta, Georgia

A procedure for the numerical solution of steady and unsteady transonic flows past a fighter wing is described. This procedure solves the three-dimensional, unsteady Euler equations in a body-fitted coordinate system. A finite-difference procedure of second-order spatial accuracy and first-order temporal accuracy is used to discretize the governing equations and a hybrid time-marching scheme is used to advance the solution from one time level to the next. In unsteady transonic flow applications involving oscillating wing surfaces, the surface motion is imposed on the solution as a transpiration boundary condition. A number of steady and unsteady calculations are presented for the F-5 fighter wing at transonic Mach numbers and detailed comparison with experiments are given.

Introduction

WITH the increased availability of supercomputers having vector processing capability and large memory, researchers have begun to look at higher-order fluid dynamics models such as the Euler and Navier-Stokes solvers to perform aerodynamic calculations for modern aircraft configurations. This trend is particularly evident in the steady-flow regime. While the transonic small-disturbance and full potential codes continue to be the primary tools for efficient aerodynamic design, aerodynamic analysis is now increasingly being done using finite-volume and finite-difference Euler codes such as the solvers described in Ref. 1. Furthermore, solvers capable of Navier-Stokes solutions for wing-alone configurations are also becoming available,[2,3] requiring the same amount of computer time (45 min to 2 h on a Cray-XMP) that was required for the full potential solvers on the slower scalar machines only a few years ago.

For a number of reasons, a similar trend has not been observed in the case of unsteady calculations. Unsteady, time-accurate calculations are inherently more expensive since relaxation techniques such as variable time steps, enthalpy damping, and grid sequencing are no longer applicable in obtaining time-accurate results. Also, several cycles in a periodic calculation will have to be made to ensure solution accuracy. This leads to large run times, particularly at very low reduced frequencies, even when a good implicit scheme is available.

Finally, three-dimensional unsteady calculations involve a number of flow parameters: Mach number, mean angle of attack, pitching and plunging motion amplitudes, mode shapes, reduced frequencies, etc. For these reasons, the aerospace industry has used the simplest nonlinear unsteady transonic aerodynamic theories (such as the LTRAN2 code) together with approximate three-dimensional corrections from such linear theories as the doublet lattice codes. Only recently have the researchers begun to use fully three-dimensional unsteady codes such as the XTRAN3 code[4,5] and the unsteady full potential solvers such as the USIPWING code[6] for practical computations. The routine use of unsteady Euler and Navier-Stokes solvers for three-dimensional aeroelastic analysis appears to be several years away, even with the availability of fast computers and improved algorithms.

Although three-dimensional Euler and Navier-Stokes solvers are not currently economical, there is a need to develop such solvers to assess the applicability of this technology in aeroelasticity. There is a need to benchmark Euler solvers using reliable experimental data, particularly for those cases where full potential and small-disturbance results already exist. Only through such a direct comparison can the efficiency and accuracy of the various competing technologies be assessed. The use of higher-order solvers will also assist in finding the solutions to the many important questions (i.e., nonuniqueness, the unsteady Kutta condition at sharp edges) that are yet to be resolved in unsteady flows, particularly at the high Mach numbers and large angles of attack. Finally, development of unsteady Euler also serves as the necessary first step in the development of unsteady Navier-Stokes solvers.

The present work addresses, at least in part, the need for time-accurate three-dimensional Euler solvers and the need for benchmark calculations using such solvers. A single configuration, viz., an F-5 fighter wing configuration, is studied using a three-dimensional time-accurate Euler solver. The Euler results are compared with some good-quality steady and unsteady experimental data[7] in order to establish the reliability and accuracy of the Euler calculations.

The mathematical and numerical formulation of the Euler solver are described briefly in the next section. The computer time and memory requirements are discussed in a separate section. Finally, a number of steady and unsteady calculations are presented and compared with experimental data.

Mathematical and Numerical Formulation

The Euler solver used in the present study is based on a solution technique recently developed for rotary wing calculations.[8] Some modifications have been made to the basic algorithm described in Ref. 11 to improve its stability characteristics.

The three-dimensional unsteady Euler equations may be written in conservation form in the Cartesian coordinate system

$$q_t + F_x + G_y + H_z = 0 \tag{1}$$

where q is the flow properties vector $\{\rho, \rho u, \rho v, \rho w, e\}$, and F, G, and H are the flux vectors along the x, y, and z directions,

Presented as Paper 85-4061 at the AIAA 3rd Applied Aerodynamics Conference, Colorado Springs, CO, Oct. 14-16, 1985; received Nov. 17, 1985; revision received Sept. 24, 1986.

*Associate Professor.
†Senior Scientist.
‡Scientist Associate.

respectively. For example, F is defined as

$$F = \begin{Bmatrix} \rho u \\ \rho u^2 + p \\ \rho uv \\ \rho uw \\ u(e+p) \end{Bmatrix} \tag{2}$$

In the above equation set, ρ is the density; u, v, and w the flow velocity components along the x, y, and z directions, respectively; e the total energy per unit volume; and p the pressure.

The Euler equations were solved in a body-fitted coordinate system (ϵ, η, ζ, τ) obtained by first constructing a sheared parabolic coordinate system around the wing and then clustering the C lines at each span station so that the first C line off the wing surface is at a constant distance of 0.01 chord from the surface. In this transformed plane, the governing equations become

$$q_\tau + F_\xi + G_\eta + H_\zeta = 0 \tag{3a}$$

The quantities q, F, G, and H are related to the flow variables $\{q\}$ and the flux vectors in the Cartesian coordinates system through the metrics of transformation. For example,

$$q = q/J$$

$$F = (\xi_t q + \xi_x F + \xi_y G + \xi_z H)/J \tag{3b}$$

The quantity J is the Jacobian of transformation and is given for the special case where y is only a function of η by

$$J = \eta_y(\xi_x \zeta_z - \xi_z \zeta_x) \tag{3c}$$

The unknown in the above system of equations is the flow property vector q. Time derivative q was discretized using two-point backward differences as $(\delta_\tau q)^{n+1}$. The spatial derivatives along the ξ and ζ directions were discretized using the following formulas:

$$F_\xi \cong \delta_\xi F$$

$$H_\eta \cong \delta_\eta H \tag{4}$$

where δ_ξ and δ_η are three-point central difference operators. The quantities F and H are nonlinear functions of q at the time level $n+1$. These functions were first linearized about the time level n. For example, F^{n+1} was written as

$$f^{n+1} = F^n + [\mathrm{D}F/\mathrm{D}q]\,(q^{n+1} - q^n) \tag{5}$$

The spanwise derivative G_η was written as a combination of the n and $n+1$ time levels. During the odd time steps, calculations were done one span station at a time, from the wing root to the outboard span station, using the latest values of the flow vector at the $(n+1)$ time level as soon as they are available. Thus, the quantity G_η was written at a typical node (i, j, k) as

$$(G^n_{j+1} - G^{n+1}_{j-1})/2$$

During the even time steps, the calculations started at the last span station outboard and progressed until the root station was reached. Then, the term G_η was discretized as

$$(G^{n+1}_{j+1} - G^n_{j-1})/2$$

Since the above differencing uses a mixture of solution vectors at the n and $(n+1)$ time levels, the above procedure is called a hybrid scheme. It may show that the use of the values at the $(n+1)$ time level as soon as they are available leads to a stable time-marching scheme, from a von Neumann analysis. The reversal of the difference scheme in the spanwise direction from one time step to the next removes any dependence that the solution may have on the sweep direction.

However, the above approach has one disadvantage. The spanwise derivatives are no longer conservative with respect to time, although they are conservative with respect to space. This fact that the spanwise derivatives are nonconservative with respect to time is not expected to affect the solution accuracy, since the streamwise and normal derivatives are all conservatively differenced.

At each of the interior points in the above discretization, the following difference equation results for the quantity $(q^{n+1} - q^n)$:

$$\left[I + \Delta t \delta_\xi \left\{\frac{\mathrm{D}F}{\mathrm{D}q}\right\}^n + \Delta t + \delta_\zeta \left\{\frac{\mathrm{D}H}{\mathrm{D}q}\right\}^n\right](q^{n+1} - q^n) = R \tag{6}$$

where for the odd time steps, the residual R is given by

$$R = -\Delta t[\delta_\xi F^n + \delta_\zeta H^n + (G^n_{j+1} - G^{n+1}_{j-1})/2] \tag{7}$$

and for the even time steps, the residual is given by

$$R = -\Delta t[\delta_\xi F^n + \delta_\zeta H^n + (G^{n+1}_{j+1} - G^n_{j-1})/2] \tag{8}$$

If pure central differences are used to discretize the spatial derivatives, it may be shown that an odd/even decoupling of the solution will occur after only a few time steps. To prevent this, and in order to remove high-frequency errors from the solution, the above finite-difference equation was modified by adding a set of artificial dissipation terms in a manner similar to that used by Pulliam and Steger.[9] To the residual R, the following fourth-order dissipation term was added:

$$R_1 = -\Delta t \epsilon_E [\delta_{\zeta\zeta\zeta\zeta} + \delta_{\eta\eta\eta\eta} + \delta_{\xi\xi\xi\xi}] J q^n \tag{9}$$

To the left-hand side operator of Eq. (6), the following implicit dissipation operators were added:

$$-\Delta t \epsilon_I J^{-1}(\delta_{\xi\xi} + \delta_{\zeta\zeta}) J \tag{10}$$

The constants ϵ_E and ϵ_I are user input coefficients. Typically, these two coefficients were set equal to 1 and 3, respectively.

After the above dissipation terms were added, the left-hand side operator appearing in Eq. (6) was approximately factored into a product of two one-dimensional operators, resulting in the following equation:

$$\left[I + \Delta t \delta_\xi \left\{\frac{\mathrm{D}F}{\mathrm{D}q}\right\}^n - \Delta t \epsilon_I J^{-1} \delta_{\xi\xi} J\right] \times \left[I + \Delta t \delta_\zeta \left\{\frac{\mathrm{D}H}{\mathrm{D}q}\right\}^n - \Delta t \epsilon_I J^{-1} \delta_{\zeta\zeta} J\right](q^{n+1} - q^n) = R + R_1 \tag{11}$$

This factored equation was solved using a series of block tridiagonal matrix inversions. The values of q at the computational boundaries were set to zero. The flow vector q at these boundaries was updated after the interior points were updated.

Boundary Conditions

At the far-field boundaries (upstream, lateral, and downstream), the flow was assumed to be undisturbed whenever the freestream Mach number was less than zero. If the freestream Mach number exceeded unity, all the five flow variables were extrapolated at the outflow boundary.

At the root span station, the Cartesian component of velocity v was set to zero. Other quantities (such as u, w, the density, and the total energy per unit volume e) were all extrapolated from the adjacent spanwise stations.

In the wake region downstream of the wing trailing edge and at the coordinate surface cut beyond the wing tip, there are two computational points corresponding to a single physical point. The flow properties on either side of this cut were obtained as averages of the flow properties above and below.

At the solid surface, the tangential components of velocity were linearly extrapolated from the interior. The density and pressure values were extrapolated similarly. For the thin wings considered here, the extrapolation of the pressure should not introduce significant errors. For thick wings with highly curved surfaces, a more accurate means of determining the surface pressure will be through the solution of the normal momentum equation at the wing surface, as is done in Ref. 9.

For steady flow calculations, the normal component of fluid velocity at the wing surface was set to zero. In unsteady flows in which the wing surface undergoes small- or large-amplitude motions, the normal component of the fluid was adjusted to account for the wing surface motion. Once the wing surface velocities x_τ, y_τ, and z_τ are known from experiments or from an aeroelastic analysis, the zero normal velocity boundary condition was enforced as

$$(u-x_\tau)\zeta_x+(v-y_\tau)\zeta_y+(w-z_\tau)\zeta_z=0 \qquad (12)$$

In the above equation, the metric coefficient must be computed using the instantaneous wing surface coordinates. Everywhere else, in the case of small wing surface deflections, the metric terms may be evaluated using the original, undeflected wing surface coordinates. When the wing surface deflections are small, it is also acceptable to neglect the grid velocity terms x_τ, y_τ, and z_τ while applying the governing equation at the interior nodes. Thus, for small-magnitude wing surface motions, the motion of the wing surface will enter into the computations only through the surface boundary condition given by Eq. (12). This concept of accounting for wing surface motion only through the boundary conditions is known as the transpiration velocity boundary condition approach.

Equation (12), along with the two tangential components of velocity at the wing surface, uniquely determines the three components of fluid velocity u, v, and w at the surface.

Advantages of the Hybrid Solution Procedure

The hybrid scheme described here has a number of advantages over existing explicit and implicit time-marching procedures, making this procedure an attractive candidate for aeroelastic analysis. Some of the desirable characteristics of the hybrid procedure are:

1) A linear stability analysis of model equations shows that the present hybrid scheme is unconditionally stable. This scheme is second-order accurate in space and first-order accurate in time.

2) It requires only two tridiagonal block matrix inversions. Conventional alternating-direction implicit (ADI) schemes require three tridiagonal matrix inversions.

3) Only one time level of storage is required. That is, only the five flow variables contained in the vector $\{q\}$ need be stored as three-dimensional arrays. The residual R and the quantity $(q^{n+1}-q^n)$ may be stored as two-dimensional arrays, since they are needed at only one span station at a time.

4) Since the solution vector q is required on only five planes at a time, the present procedure may be coded for efficient memory utilization on virtual memory machines such as the CDC Cyber 205 computer.

As discussed earlier, the present procedure uses a non-conservative time differencing, while evaluating the spanwise derivatives in the Euler equations. Although such a non-conservative time differencing may be expected to yield incorrect shock speeds, the unsteady calculations performed using this solver show no loss in solution accuracy, at least in the limited number of calculations done with this solver.

Results and Discussion

The Euler calculations were all done on a $121\times16\times21$ grid, with 90 points on the airfoil at each span station (45 above and

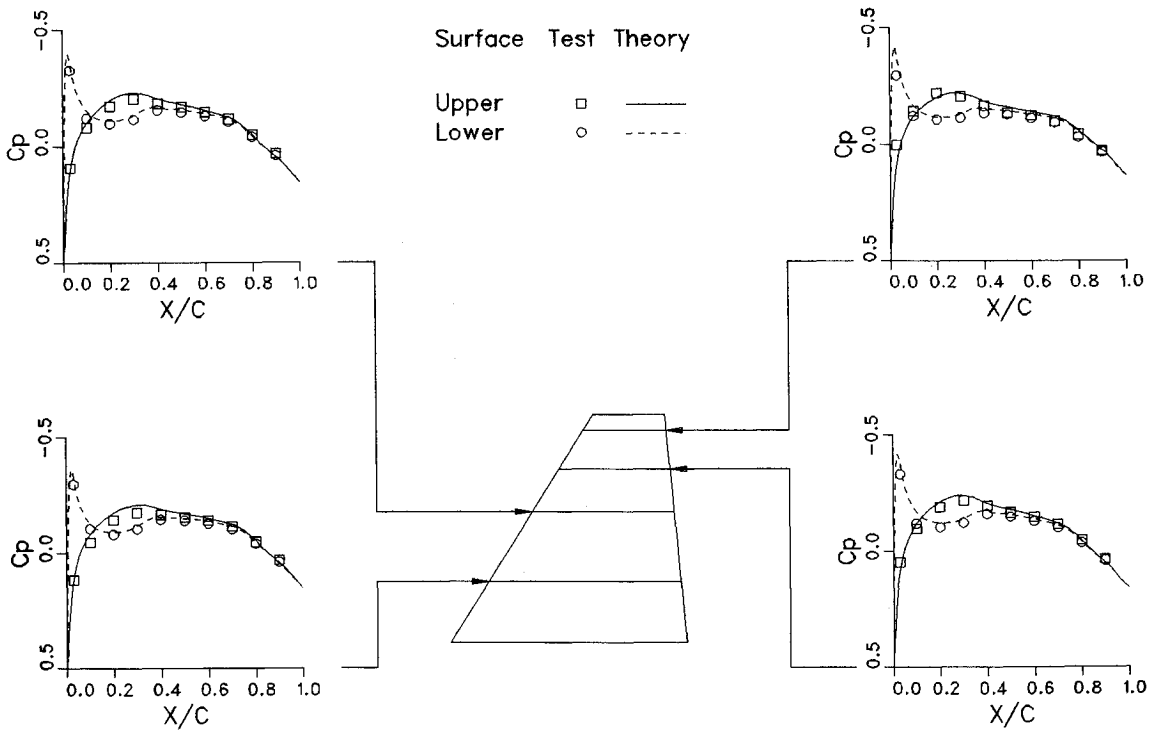

Fig. 1 Steady flow past the F-5 wing at 0.80 Mach number, zero angle of attack.

45 below). In the span direction, there were 11 span stations on the wing and 5 additional stations beyond the wing tip. A constant time step value of 0.005–0.007 was used in these calculations. These values are nondimensionalized by the ratio between the user input reference length and the freestream speed of sound. Since the smallest grid spacing on the sheared parabolic grid was equal to 0.000072 units, the above range of time steps correspond to a CFL number of 100 or more.

An F-5 clean wing configuration was chosen for detailed study. This case was chosen because a large set of experimental steady and unsteady data are available for this wing.[7] Unsteady small-disturbance[5] and full potential results[6,10] are also available for this wing. In addition, the small aspect ratio, the large leading-edge sweep, and the large taper ratio of the planform make this wing a difficult but interesting configuration to study. In this work, only the Euler results are presented. The reader interested in direct one-to-one comparisons between the full potential and Euler solvers is referred to Ref. 11 for such comparisons.

Steady Flow Results

The following steady flow calculations were performed. These solutions were obtained by solving the unsteady Euler equations in a time-accurate manner until the flow properties and integrated air loads converged. Cases considered were: A) Mach number 0.80, zero angle of attack; B) Mach number 0.95, zero angle of attack; and C) Mach number 1.35, 0.5-deg angle of attack.

The Euler solutions for the above three cases are shown in Figs. 1–3 at selected span stations along with the experimental data. In general, the predictions of the Euler solver are in favorable agreement with the experiments. At the Mach number of 0.8, where no noticeable shocks exist, the experiments and the Euler solver show nearly identical surface pressures. The slightly drooped leading edge of the wing produces large pressure spikes at the wing leading edge, which is well predicted by the Euler solver. At Mach number 0.95, the Euler solver produced shocks that were slightly downstream of the experimental data. The shocks are also somewhat stronger than those observed in the experiments. The inclusion of turbulent boundary-layer effects should improve the agreement between the theory and the experiment further. A small overshoot upstream of the shocks was also observed in the Euler solutions. This overshoot is caused by the use of fourth-order dissipation terms in the vicinity of the shock waves and may be removed through the use of second-order dissipation terms near shocks. Since an abrupt switching of dissipation terms from one form to another may result in a nonconservative form of the discretized equations and incorrect shock locations, such a switching must be carefully done.

The Euler solver yielded a stable, converged numerical solution in all the cases, including the case where the freestream was supersonic. The time steps used for cases A, B, and C were 0.007, 0.005, and 0.003, respectively, when normalized with respect to the user input reference length and the freestream speed of sound.

The effect of grid density on the converged solution was examined by solving case A on a $81 \times 12 \times 18$ coarse grid. The results for the coarse grid may be found in Ref. 8. While features such as the pressure peaks at the leading edge were all predicted accurately on the coarse grid, the the Euler solver predicted a somewhat smeared shock pattern on the coarser grid.

The supersonic freestream case was also computed using a three-dimensional full potential solver.[11] The full potential results are shown in Fig. 4. A comparison of the Euler results and the full potential results revealed some small oscillations in the Euler surface pressure solutions in the vicinity of the sonic line. Similar oscillations were not observed at the subsonic freestream Mach numbers. It is believed that these oscillations may be removed through the use of improved artificial dissipation forms.

Unsteady Results

The following case was considered: D) Mach number 0.8, zero angle of attack, 0.113 deg amplitude pitching oscillations at a frequency of 40 Hz.

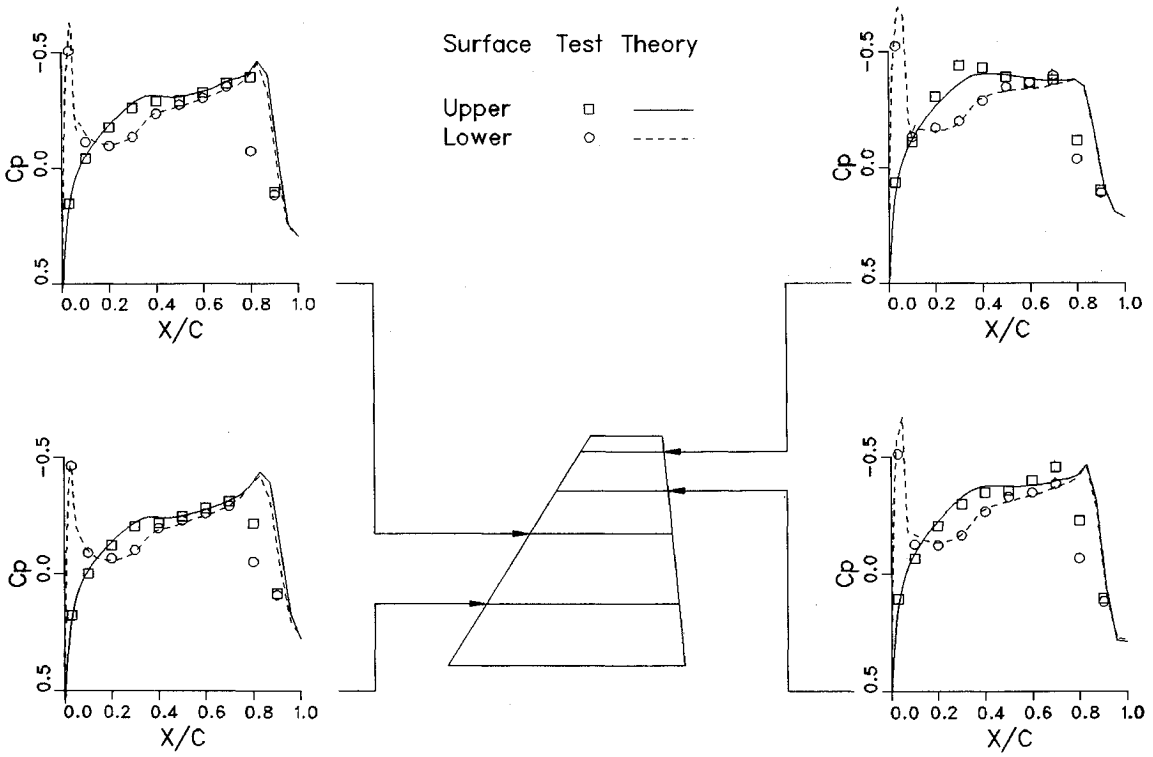

Fig. 2 Steady flow past the F-5 wing at 0.95 Mach number, zero angle of attack.

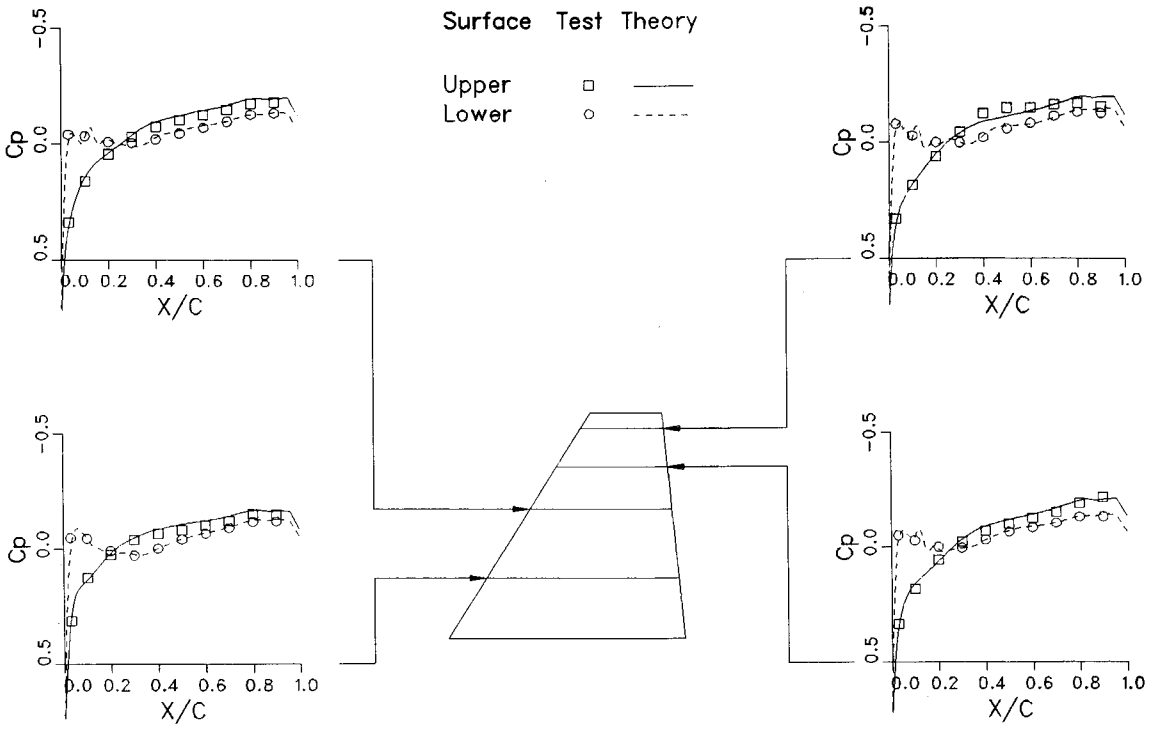

Fig. 3 Steady flow past the F-5 wing at 1.35 Mach number, 0.5-deg angle of attack.

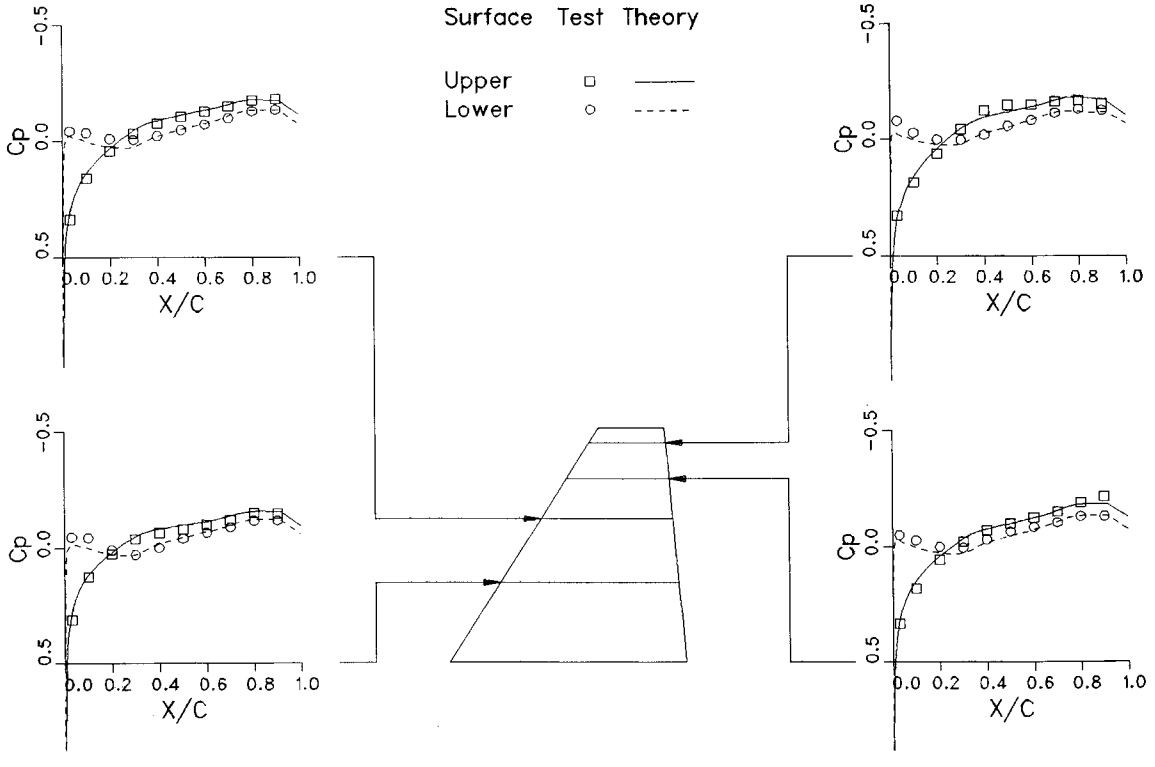

Fig. 4 Steady potential flow solution for the F-5 wing at 1.35 Mach number, 0.5-deg angle of attack.

The computed unsteady pressure distributions at 0, 90, 180, and 360 deg of phase were used to estimate the real (in-phase) and out-of-phase components of the surface pressure coefficients. A linear interpolation of the computed surface distributions was needed to obtain the pressure values at the span locations where experimental data are available. These values are plotted in Figs. 5 and 6 and compared with the experimental data. Again, a very good agreement with the experimental data is found. Near the leading edge, the Euler solver predicts slightly higher suction levels for the real (in-phase) part of the surface pressure. This may be improved by the use of a boundary-layer scheme that accounts for the viscous effects. The change in the sign of the out-of-phase pressure component downstream of the quarter-chord line is also predicted accurately.

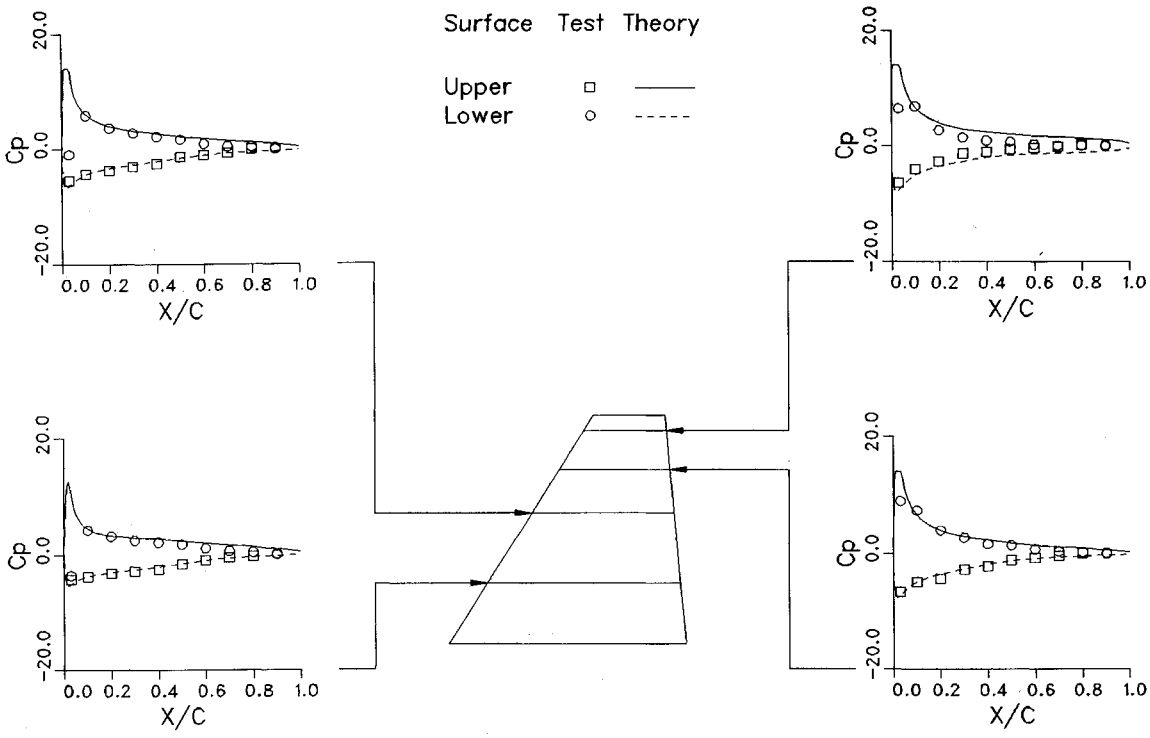

Fig. 5 Unsteady flow past the F-5 wing oscillating in pitch at Mach number 0.8 and zero mean angle of attack showing in-phase component of the surface pressure distribution.

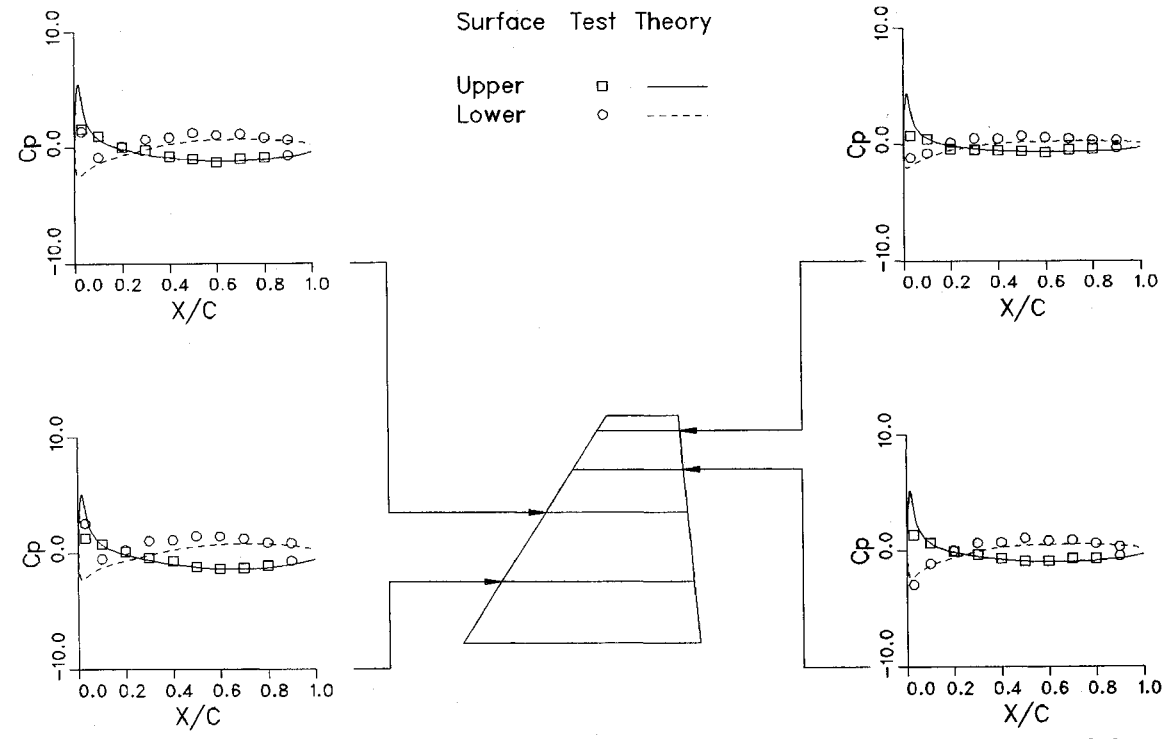

Fig. 6 Unsteady flow past the F-5 wing oscillating in pitch at Mach number 0.8 and zero mean angle of attack showing out-of-phase component of the surface pressure distribution.

Conclusions

The suitability of using higher-order flow models based on the unsteady Euler equations in aeroelastic applications was examined by computing the steady and unsteady flows past an F-5 wing. As may be expected, for the small angles of attack and the low transonic Mach numbers encountered here, the Euler solver gave results that are in quantitative agreement with the experiments. Some improvements are needed in the artificial dissipation terms used in the Euler solver to remove the small overshoots and wiggles that occur near shocks and sonic lines. It also appears that the discrepancies between the experiments and the theory may be reduced by the use of an integral boundary-layer scheme to account for the viscous displacement effects.

For the limited number of calculations performed here, the above calculations also indicate that the unsteady Euler solver

is robust enough and accurate enough to be used in aeroelastic calculations. The present authors' experience with the unsteady full potential solvers indicates that the full potential solver is about five times cheaper than the Euler solver per point per time step. Thus, full potential solvers such as the ones described in Ref. 6 are likely to be the primary tools in aeroelastic analysis. The Euler solver can, however, be used in difficult cases involving stronger shocks and large local Mach numbers and may also be used to obtain an independent check of the potential flow results in selected cases.

Acknowledgments

The three-dimensional Euler solver described here was developed at the Georgia Institute of Technology. The unsteady Euler calculations reported here were supported by the Lockheed Georgia Company under the Independent Research and Development Program.

References

[1]Jameson, A. and Baker, T. J., "Multigrid Solutions of the Euler Equations for Aircraft Configurations," AIAA Paper 84-0093.

[2]Agarwal, R. K. and Deese, J. E., "Computation of Transonic Viscous Airfoil, Inlet and Wing Flow Fields," AIAA Paper 84-1551.

[3]Holst, T. L., Kaynak, U., Gundy, K. L., Thomas, S. D., and Flores, J., "Numerical Solution of Transonic Wing Flow Fields Using an Euler/Navier-Stokes Zonal Approach," AIAA Paper 85-1640.

[4]Borland, C. J. and Rizzetta, D. P., "Transonic Unsteady Aerodynamics for Aeroelastic Applications," AFWAL TR-80-3107, May 1982.

[5]Borland, C. J. and Sotomayer, W. A., "An Algorithm for Unsteady Transonic Flow about Tapered Wings," AIAA Paper 84-1567.

[6]Malone, J. B., Sankar, L. N., and Sotomayer, W. A., "Unsteady Aerodynamic Modeling of a Fighter Wing in Transonic Flow," *Journal of Aircraft*, Vol. 23, Aug. 1986, pp. 611–620.

[7]Tijdeman et al., "Transonic Wind Tunnel Tests on an Oscillating Wing with External Stores," AFFDL-TR-78-194, Dec. 1978.

[8]Sankar, L. N., Wake, B. E., and Lekoudis, S. G., "Solution of the Unsteady Euler Equations for Fixed and Rotary Wing Configurations," *Journal of Aircraft*, Vol. 23, April 1986, pp. 283–290.

[9]Pulliam, T. H. and Steger, J. L., "On Implicit Finite-Difference Simulations of Three-Dimensional Flow," *AIAA Journal*, Vol. 18, Feb. 1980, pp. 159–167.

[10]Malone, J. B. and Sankar, L. N., "Application of a Three-Dimensional Steady and Unsteady Full Potential Method for Transonic Flow Computations," AFWAL-TR-84-3011, May 1984.

[11]Sankar, L. N., Malone, J. B., and Schuster, D., "Full Potential and Euler Solutions for the Unsteady Transonic Flow Past a Fighter Wing," AIAA Paper 85-4061, Oct. 1985.